An Overview of Novel Tetragonal Oxides with Enhanced High-Temperature Capabilities for Structural Applications

Liu Qu[1], Kwang-Leong Choy[2]*

UCL Institute for Materials Discovery, University College London, London, WC1E 7JE, UK

Abstract— *Tetragonal oxides possess great potential in structural applications because of the superior thermomechanical properties and corrosion resistance. This paper presents an overview of the structure and thermal properties of (Dy, Ce, Y)-doped ZrO_2. The tetragonal structure is enhanced by doping Ce^{4+} cations to YSZ, whereas doping Dy^{3+} stabilizes the cubic phase. In comparison to conventional 8 wt.% Y_2O_3 stabilized ZrO_2 (equivalent to 4 mol% Y_2O_3 stabilized ZrO_2, 4YSZ), the thermal conductivity of 3Dy5Ce-YSZ and 2Dy-YSZ is decreased and the coefficient of thermal expansion (CTE) is increased, which are desirable for thermal barrier materials. The potential of Dy and Ce doped 4YSZ as thermal barrier materials for high-temperature applications has been highlighted in the paper.*

Keywords— thermal barrier coating materials, tetragonal structure, thermal conductivity, coefficient of thermal expansion

I. INTRODUCTION

Structural oxides that exhibit low thermal conductivity, high corrosion resistance, high thermal shock resistance, high melting point, and high CTE are utilized as thermal barrier coatings (TBCs) in gas turbines for example, to protect the hot-sections from high-temperature gases [1]. TBCs comprise of a bond coat, thermally grown oxide (TGO) layer (e.g. α-Al_2O_3) and ceramic top coat [2]. The harsh operating environments of TBCs include high temperatures, high pressures, oxidative and corrosive conditions, and thermal cycling process, bringing about challenging requirements for novel material compositions [3]. The deposition of TBCs on the hot-section components contributes to the decrease of their surface temperature and thus enhances the fuel efficiency of the high-temperature applications.

Tetragonal oxides, such as doped ZrO_2 with rare earth elements (e.g. Dy^{3+} and Sc^{3+}) are reported to have lower thermal conductivity and enhanced CTE, as compared with conventional 8 wt.% YSZ [4, 5]. In contrast to the cubic structure, tetragonal 4YSZ shows higher fracture toughness attributed to the tetragonal-monoclinic transformation, contributing to the superior erosion and impact resistance [6, 7]. The thermochemical compatibility between 4YSZ and Al_2O_3 is high during the thermal cycling process, while the pyrochlore oxide is reported to react with Al_2O_3 forming new phases at high temperatures [8].

Although the thermal conductivity and sintering characteristics of Dy-YSZ coatings have been studied [4, 9], to our best knowledge, no apparent work has been reported on the structure, thermal conductivity and CTE of (Dy, Ce)-YSZ. This paper investigates the correlation between compositional variation and crystal structure of Dy^{3+} and Ce^{4+}doped YSZ. It was discovered that the addition of Ce^{4+} to ZrO_2 stabilized the tetragonal structure, and the thermal conductivity was reduced by 29%. Moreover, Dy^{3+} incorporation to ZrO_2 reduced the thermal conductivity and stabilized the cubic phase [4].

II. STRUCTURE

The phase composition was characterized by XRD, and the results are shown in Figure 1. 4 YSZ and 2Dy-YSZ consist of the cubic and tetragonal structures, whereas no cubic phase is identified in the XRD pattern of 3Dy5Ce-YSZ. The desired phase for 4YSZ is the t'-tetragonal structure [2, 10, 11]. In this case, the incorporation of Dy^{3+} stabilizes the cubic phase, as the peak intensity of the cubic (311) of 2Dy-YSZ is increased, compared with that of 4YSZ (Figure 2). By contrast, the XRD pattern of 3Dy5Ce-YSZ exhibits tetragonal (103) and (211) double-peak and no peaks from other phases are observed. Hence, doping trivalent Dy^{3+} to ZrO_2 stabilizes the cubic phase, whereas the addition of Ce^{4+} stabilizes the tetragonal phase.

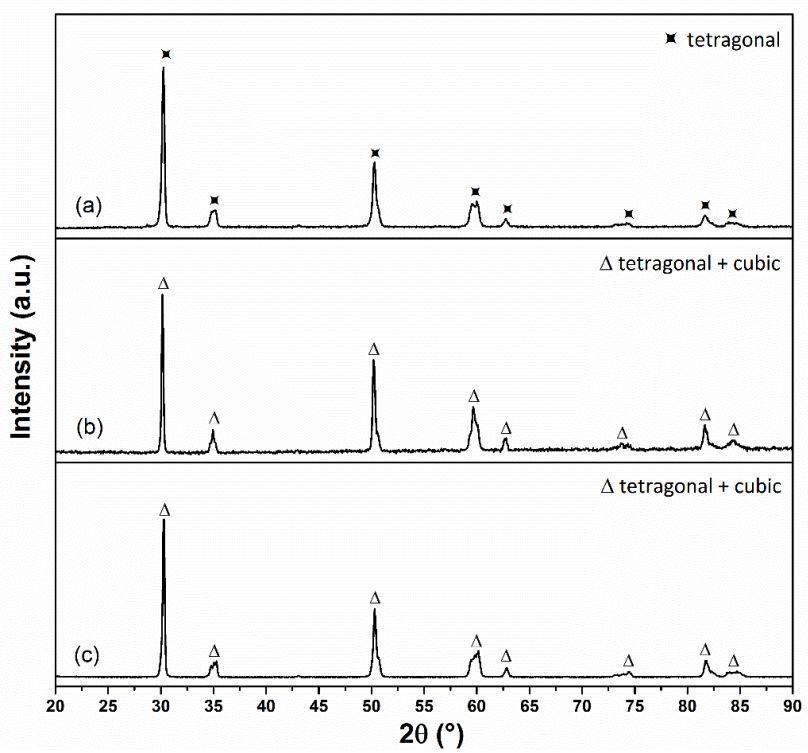

FIGURE 1. XRD PATTERNS OF (DY, CE)-YSZ: (A) 3DY5CE-YSZ; (B) 2DY-YSZ; (C) 4YSZ

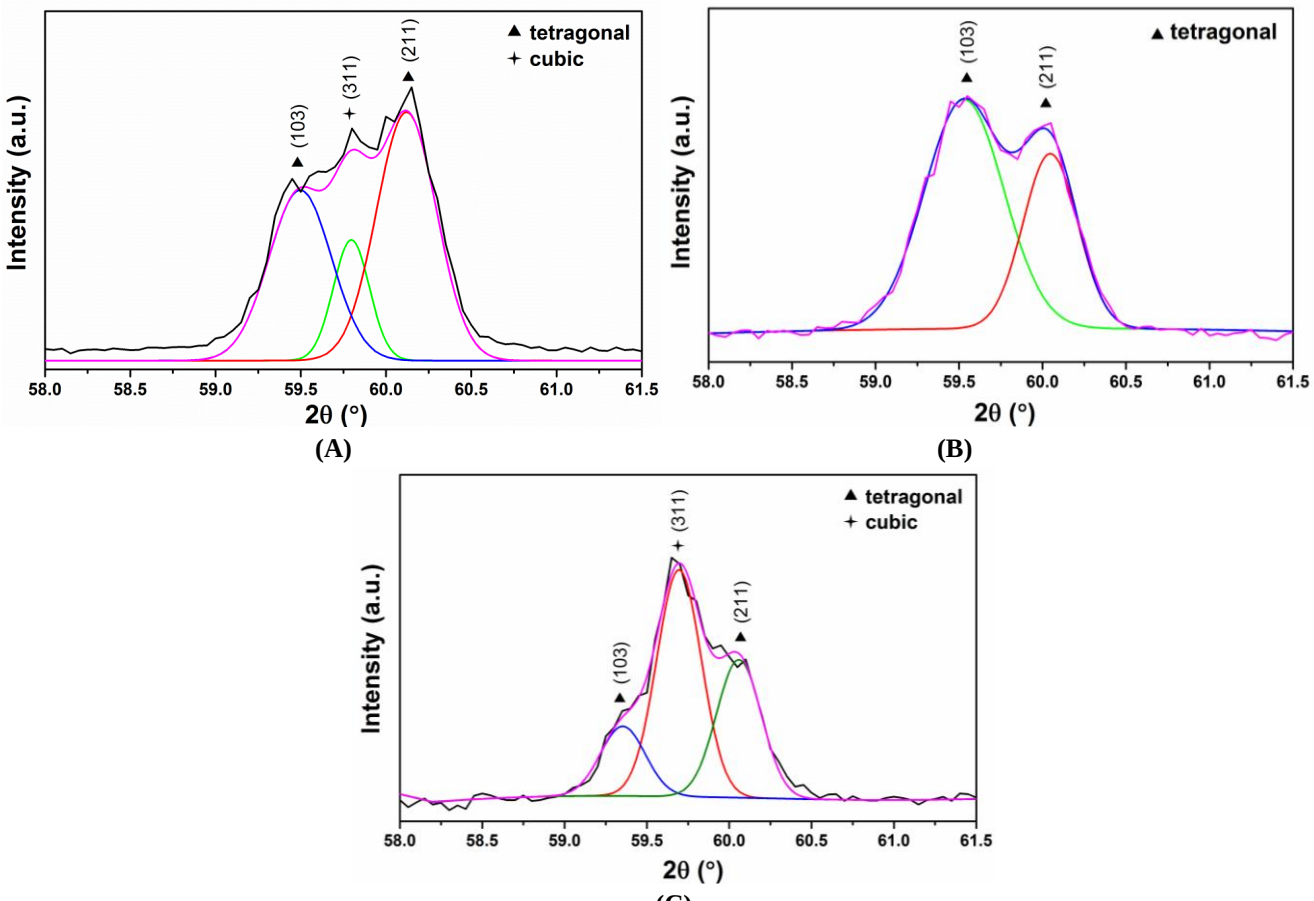

FIGURE 2. XRD PATTERNS OF (DY, CE)-YSZ AT 2θ BETWEEN 58° AND 61.5°: (A) 4YSZ; (B) 3DY5CE-YSZ; (C) 2DY-YSZ

The Raman spectra of (Dy, Ce)-YSZ are shown in Figure 3. Five active vibrational modes from 200 cm^{-1} to 800 cm^{-1} represent the characteristic Raman wavenumbers of the tetragonal oxide (labeled I_2 to I_6). For 4YSZ, the peak at 259 cm^{-1} represents the O-Zr-O E_g stretching mode; 324 $cm^{-1}$is the Zr-O B_{1g} bending mode; 464 cm^{-1} corresponds to the Zr-O stretching E_g mode; 612 cm^{-1} is assigned as the symmetric O-Zr-O A_{1g} stretching mode; 641 cm^{-1} is the asymmetric O-Zr-O E_g stretching mode [12].

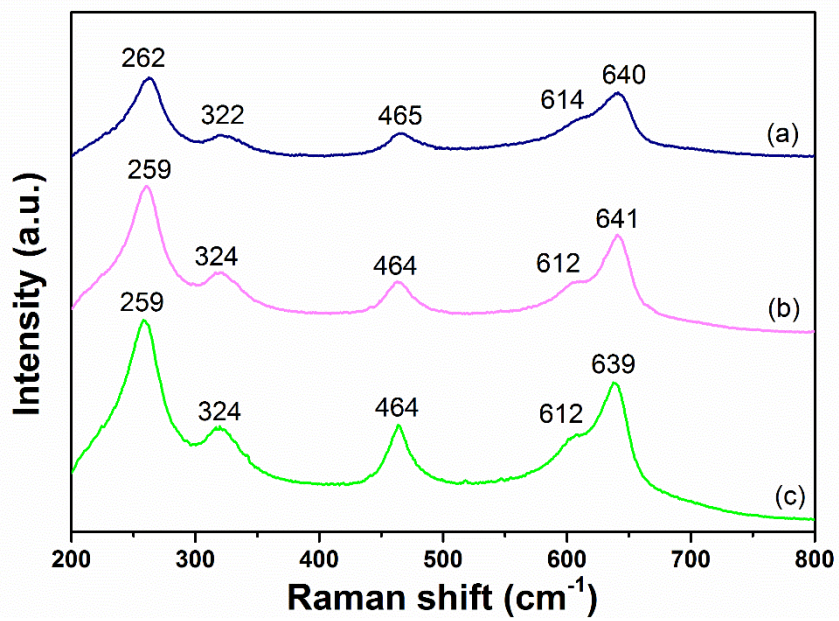

FIGURE 3. RAMAN SPECTRA OF: (A) 2DY-YSZ; (B) 4YSZ; (C) 3DY5CE-YSZ

The oxygen displacement along the *c*-axis in a tetragonal lattice can be described by the relative intensity ratio between the third and fifth peaks (I_4/I_6) [13]. The intensity ratio of $I_4/I_6$was calculated and presented in Table 1. The addition of Dy^{3+} to YSZ decreased I_4/I_6, whereas the incorporation of Ce^{4+} enhanced I_4/I_6. The oxygen displacement in 2Dy-YSZ was decreased, whereas it was increased in 3Dy5Ce-YSZ, as compared with that in 4YSZ.

TABLE 1
INTENSITY RATIO (I_4/I_6) OF RAMAN SPECTRA

	4YSZ	2Dy-YSZ	3Dy5Ce-YSZ
I_4/I_6	0.5757	0.3631	0.7170

III. THERMAL CONDUCTIVITY

The thermal conductivity of ceramic oxides is controlled by the lattice vibration namely the phonon scattering and electromagnetic radiation namely the photon scattering [14]. Lower thermal conductivity can be achieved by the incorporation of lattice defects such as the vacancy and interstitial atoms to enhance the phonon scattering. The thermal conductivity of tetragonal 4YSZ is reported to be 2.3-3.0 W/m·K and the CTE is 11×10^{-6} $°C^{-1}$[2, 15-17]. Doping rare earth oxides to the ZrO_2 creates the mass and ionic radii differences, strongly enhancing the phonon scattering and decreasing the lattice thermal conductivity. The measured thermal conductivity was converted to that of a dense sample using Equation 1 [18]. The thermal conductivity values of 2Dy-YSZ (2.8031 $\pm$ 0.1657 W/m·K) and 3Dy5Ce-YSZ (2.6063 $\pm$ 0.2717 W/m·K) are lower than that of 4YSZ (3.6469 $\pm$ 0.1031 W/m·K) by 23% and 29%, respectively. The atomic weight of Dy^{3+} (162.5 g/mol, and Ce^{4+} (140.116 g/mol) and Y^{3+} (88.9 g/mol) is higher than that of Zr^{4+} (91.22 g/mol) [19]. The values of ionic radius of Dy^{3+} (1.03 Å), Ce^{4+} (0.97 Å), and Y^{3+} (1.02 Å) are larger than that of Zr^{4+} (0.84 Å)[19]. The formation of such lattice defects results in the lattice distortion and increases the lattice vibration, hence decreasing the phonon mean free path and thermal conductivity. Such decrease of the thermal conductivity would allow higher engine operation temperature and higher thermal efficiency of an aero engine.

IV. COEFFICIENT OF THERMAL EXPANSION

The CTE of (Dy, Ce)-YSZ is shown in Figure 4. Doping Dy^{3+} and Ce^{4+} cations to 4YSZ enhances the CTE at the high-temperature range. The increase of the CTE is a result of the ionic radii misfit of Dy^{3+}, Ce^{4+}, Y^{3+} and Zr^{4+}, which can weaken the atomic bond. Moreover, the values of bonding energy of Dy-O (615 kJ/mol) and Y-O (714.4 kJ/mol) are lower than that of Zr-O (766 kJ/mol), contributing to the higher CTE of (Dy, Ce)-YSZ[19]. Furthermore, as the phase composition of 2Dy-YSZ and 4YSZ consisting of both cubic and tetragonal structures, their lattice disorder would be higher than that of tetragonal 3Dy5Ce-YSZ. Although the larger bonding energy of Ce-O (790 kJ/mol) than that of Zr-O and Dy-O is likely to decrease the CTE, the larger ionic radius of Ce^{4+} (0.97 Å) results in the lattice distortion and thus enhances the CTE.A higher CTE is preferable for ceramic top coat during thermal cycling process, when high thermal expansion mismatch results in residual stresses and hence decreases its high-temperature capabilities.

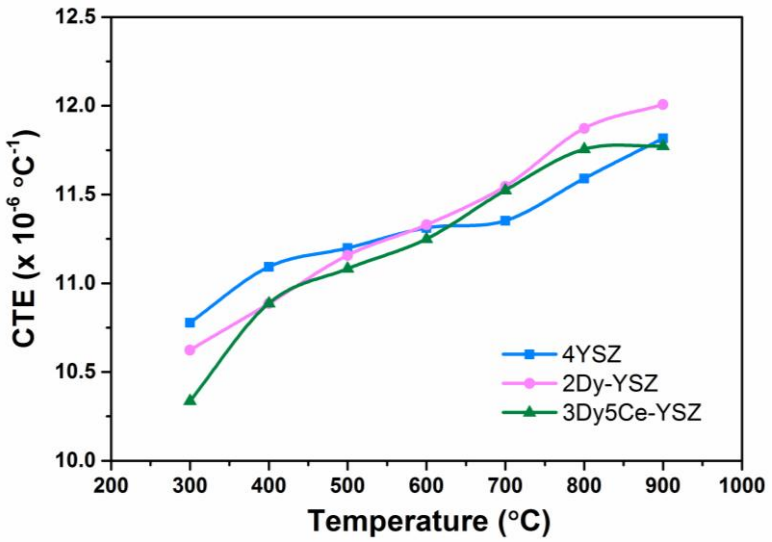

FIGURE 4. COEFFICIENT OF THERMAL EXPANSION OF (DY, CE)-YSZ

The incorporation of $Ce^{4+}$to YSZ facilitates the formation of the tetragonal structure, whereas adding Dy^{3+} enhances the cubic phase. The decrease of the thermal conductivity attributed to the addition of Ce^{4+} and Dy^{3+} was achieved by 29%, as compared with that of 4YSZ. Although doping Ce^{4+} does not create the oxygen vacancy, the mass and atomic radius differences can effectively increase the phonon scattering and phonon mean free path. The combinational effects of doping Dy^{3+} and Ce^{4+} can bring about more lattice distortion and defects, significantly weakening the atomic bond and enhancing the dilation against temperature. Moreover, the thermomechanical properties of tetragonal structures are superior to those of cubic oxides, contributing to their great potential in structural applications [20]. The fracture toughness of tetragonal YSZ is reported to be higher than that of cubic YSZ, resulting from the ferroelastic toughening at high temperatures [7]. In comparison with other structures such as the pyrochlore structure, the thermochemical compatibility of the doped YSZ is reported to be stable at higher temperatures [4].

V. CONCLUSION

In conclusion, Dy-YSZ shows cubic and tetragonal structures, while (Dy, Ce)-YSZ exhibits the tetragonal structure. The oxygen displacement in the tetragonal lattice is increased by doping Ce^{4+} in contrast to the incorporation of Dy^{3+} cations to YSZ. The thermal conductivity of 2Dy-YSZ and 3Dy5Ce-YSZ is lower than that of 4YSZ. The CTE values of 2Dy-YSZ and 3Dy5Ce-YSZ are enhanced as compared with undoped 4YSZ. These novel tetragonal oxides show great potential in the high-temperature structural applications such as TBCs, ascribed to their lower thermal conductivity and improved CTE.

VI. METHODS

Starting materials are 4 mol% YSZ, CeO_2 and Dy_2O_3. The powders of CeO_2, Dy_2O_3 and 4YSZ were mixed in desired stoichiometric ratios, followed by ball milling to achieve the homogeneity. The powders were isostatically pressed into pellets at room temperature. The bulk sample for (Dy, Ce, Y)-doped ZrO_2 were sintered at 1300°C for 6 hours, and (Dy, Y)-doped ZrO_2 and 4YSZ pellets were sintered at 1400°C for 6 hours.

The crystal structure of (Dy, Ce)-YSZ was characterized using X-ray diffractometer (Siemens D500, Cu-Kα radiation) and Raman spectroscopy (Olympus BX41, He-Ne laser source 632.8 nm). The thermal conductivity was measured using a TCi thermal conductivity analyzer (C-Therm Technologies). The density was calculated based on the mass and volume of the pellet, from which the porosity of the sample was determined. The thermal conductivity of the fully dense sample was determined by,

$$\kappa_0 = \frac{3}{3-4\varphi}\kappa, \quad (1)$$

where φ is the porosity, κ_0 is the corrected thermal conductivity for fully dense materials and κ is the measured thermal conductivity [18]. The CTE was measured by a NETSZCH DIL 402C dilatometer from room temperature to 900°C with a

REFERENCES

[1] X. Cao, R. Vassen, D. Stoever, *Journal of the European Ceramic Society*, **24**, 1, (2004), 1-10.
[2] N.P. Padture, M. Gell, E.H. Jordan, *Science*, **296**, (2002), 280-284.
[3] R. Vassen, Y. Kagawa, R. Subramanian, P. Zombo, D. Zhu, *MRS Bulletin*, **37**, 10, (2012), 911-916.
[4] L. Qu, K.-L. Choy, *Ceramics International*, **40**, 8, (2014), 11593-11599.
[5] H. Liu, S. Li, Q. Li, Y. Li, *Materials and Design*, **31**, (2010), 2972-2977.
[6] J. Chevalier, L. Gremillard, *Journal of the American Ceramic Society*, **92**, 9, (2009), 1901-1920.
[7] R. Darolia, *International Materials Reviews*, **58**, 6, (2013), 315-348.
[8] R.M. Leckie, S. Krämer, M. Rühle, C.G. Levi, *Acta Materialia*, **53**, 11, (2005), 3281-3292.
[9] Y.J. Wang, in: Applied Science, The University of British Columbia (Vancouver), 2009, 90.
[10] R. Vassen, X. Cao, F. Tietz, D. Basu, D. Stover, *Journal of the American Ceramic Society*, **83**, (2000), 2023-2028.
[11] K.H. Stern, Metallurgical and ceramic protective coatings, Chapman and Hall, 1996.
[12] S. Heiroth, R. Frison, J.L.M. Rupp, T. Lippert, E.J. Barthazy Meier, E. Müller Gubler, M. Döbeli, K. Conder, A. Wokaun, L.J. Gauckler, *Solid State Ionics*, **191**, 1, (2011), 12-23.
[13] C. Viazzi, J.-P. Bonino, F. Ansart, A. Barnabé, *Journal of Alloys and Compounds*, **452**, 2, (2008), 377-383.
[14] P.G. Klemens, M. Gell, *Materials Science and Engineering A*, **245**, (1998), 143-149.
[15] J. Wu, X. Wei, N.P. Padture, P.G. Klemens, M. Gell, E. García, P. Miranzo, M.I. Osendi, *Journal of the American Ceramic Society*, **85**, 12, (2004), 3031-3035.
[16] H. Lu, C.-A. Wang, C. Zhang, *Journal of the American Ceramic Society*, **96**, 4, (2013), 1063-1066.
[17] J.-F. Bisson, D. Fournier, M. Poulain, O. Lavigne, R. Mévrel, *Journal of the American Ceramic Society*, **83**, 8, (2000), 1993-1998.
[18] K.W. Schlichting, N.P. Padture, P.G. Klemens, *Journal of Materials Science*, **36**, (2001), 3003-3010.
[19] D.R. Lide, W.M. Haynes, CRC handbook of chemistry and physics: a ready-reference book of chemical and physical data, CRC Press, Taylor and Francis Group, 2009.
[20] C. Mercer, J.R. Williams, D.R. Clarke, A.G. Evans, *Proceedings of the Royal Society A*, **463**, (2007), 1393-1408.